

Creating local contrast in small-angle neutron scattering by dynamic nuclear polarization

B. van den Brandt,^b H. Glättli,^c P. Haulte,^b J. Kohlbrecher,^{a*} J. A. Konter,^b A. Michels,^d H. B. Stuhmann^e and O. Zimmer^f

^aLaboratory for Neutron Scattering, ETH Zurich, and Paul Scherrer Institut, CH-5232 Villigen PSI, Switzerland,

^bLaboratory for Developments and Methods, Paul Scherrer Institut, CH-5232 Villigen PSI, Switzerland, ^cService de Physique de l'Etat Condensé (CNRS URA 2464), CEA Saclay, 91191 Gif-sur-Yvette Cedex, France,

^dTechnische Physik, Universität des Saarlandes, Saarbrücken, Germany, ^eInstitut de Biologie Structurale Jean-Pierre Ebel, CEA/CNRS/UJF, F-38027 Grenoble Cedex 1, France, and ^fTechnische Universität München, James-Frank-Strasse, D-85748 Garching, Germany. Correspondence e-mail: joachim.kohlbrecher@psi.ch

Low-resolution small-angle neutron scattering measurements can benefit from polarized protons to generate scattering contrast profiles. In a recently developed technique, time-resolved polarized SANS tries to make use of spatial polarization gradients created around paramagnetic centres at the onset of dynamic nuclear polarization. The time constants which describe the build-up of polarization around the paramagnetic centre and the subsequent diffusion of polarization in the solvent were determined by analysing the temporal evolution of the nuclear polarization. The possible use and the limitations of this technique as a spectroscopic tool are discussed.

© 2007 International Union of Crystallography
Printed in Singapore – all rights reserved

1. Introduction

Dynamic nuclear polarization (DNP) is an efficient tool for creating scattering contrast in homogeneous samples exploiting the strong spin dependence of thermal neutron scattering on protons. In materials containing a sufficient concentration of hydrogen, the scattering-length density can be changed remarkably by polarizing the hydrogen nuclei. By using DNP, a nuclear polarization far beyond the Boltzmann value can be created. A necessary prerequisite for this technique is the existence of unpaired electrons (paramagnetic centres) in the sample. At temperatures around $T = 1$ K and at magnetic fields of $B \geq 2.5$ T the polarization of the electron spin is close to unity. On irradiation with microwaves of frequency close to the electron paramagnetic resonance frequency, the polarization of the electron spins can be transferred to the nearby nuclei, taking advantage of the dipolar interaction between the electrons and the nuclear spins. This interaction falls off with the third power of the distance between electron and nucleus, so that nuclei close to the paramagnetic centre are polarized first, while far-away nuclei rely on spin diffusion to reach equilibrium. The DNP mechanism therefore does not *a priori* lead to a homogeneous polarization distribution. Situations can be imagined in which domains of highly polarized protons around paramagnetic centres survive long enough to produce a contrast which can be detected by neutron scattering. According to this simplified two-step polarization model the question arises as to whether it would be possible to create spatial polarization gradients around paramagnetic centres at the onset of DNP. Such polarization domains could considerably enhance the scattering amplitude of *e.g.* free radicals and thus contribute to the determination of their positions inside a complex molecule. However, a significant gradient of polarization can only be achieved if the spin diffusion is slow enough compared to the efficiency of the DNP process for nuclei close to paramagnetic centres.

Despite considerable theoretical and experimental work, mainly based on the one-centre model sketched above, this mechanism is not

yet fully understood. Experiments to elucidate the DNP mechanism on a microscopic level are missing. We have therefore developed experimental techniques sensitive to the proton polarization and relaxation dynamics on time and length scales encountered in substances frequently used for polarized targets. We established a combination of stroboscopic time-resolved small-angle neutron scattering with continuous-wave nuclear magnetic resonance (cw-NMR) synchronized to cyclic microwave irradiation. The first successful experiments have been carried out on $\text{Na}(\text{C}_{12}\text{H}_{20}\text{O}_7\text{Cr}^{\text{V}})\text{H}_2\text{O}$ (EHBA–Cr^V) complexes dissolved in deuterated glycerol–water mixtures with different small ¹H concentrations. We have extended these studies to $(\text{C}_{32}\text{H}_{66}\text{O}_{11})_{56}$ (C12E10) micelles doped with the nitroxyl radical 2,2,6,6-tetramethylpiperidine-1-oxyl (TEMPO) and to undoped polystyrene nanospheres of 80 nm radius embedded in a protonated glycerol–water mixture which is doped with EHBA–Cr^V complexes. The nanospheres are thought to act as an exclusion volume for the EHBA–Cr^V complexes to get protonated areas free of polarization centres. In this last system it was possible to directly see a time-dependent polarization gradient.

2. Choice of samples and their preparation

We have successfully performed nuclear spin-dependent small-angle neutron scattering (SANS) experiments on three different classes of samples where the structure giving rise to a SANS signal differs significantly in size from one class to the other.

(1) We started our investigations with frozen solutions of $\text{Na}(\text{C}_{12}\text{H}_{20}\text{O}_7\text{Cr}^{\text{V}})\text{H}_2\text{O}$ (EHBA–Cr^V) paramagnetic centres in glycerol–water mixtures (van den Brandt *et al.*, 2002, 2004, 2006). The EHBA–Cr^V molecule has a radius of about 0.5 nm, where the Cr^V carries the unpaired electron. The deuteration of the solvent mixtures was varied between 80 and 98% and the EHBA–Cr^V concentration was chosen between 1.25×10^{19} and 5.0×10^{19} cm⁻³. In these model

samples the EHBA-Cr^V complex, whose unpaired electrons are surrounded by 22 ¹H atoms (the so-called close protons), is embedded in a partially deuterated matrix with a chosen concentration of ¹H atoms (giving the bulk protons). As a consequence of the relatively small size of the EHBA-Cr^V molecule, the nuclear polarization build-up around paramagnetic centres during DNP gives rise to a coherent nuclear spin-dependent SANS signal only at relatively high Q values ($Q > 1\text{--}2\text{ nm}^{-1}$), which lie at the limit of what can be seen with conventional SANS instruments. [Here Q is the modulus of the scattering vector, defined as $Q = |\mathbf{Q}| = (4\pi/\lambda)\sin(\theta/2)$, with λ being the neutron wavelength and θ being the scattering angle.] Moreover, the ratio of interesting coherent signal to incoherent background was relatively low in these samples.

(2) In an attempt to improve this situation, we prepared samples where the paramagnetic centres are incorporated into a much larger protonated host molecule. As host molecules we used C12E10 [(C₃₂H₆₆O₁₁)₅₆] micelles with an approximate radius of about 2.6 nm which could be doped with 2,2,6,6-tetramethylpiperidine-1-oxyl (TEMPO) nitroxyl radicals. The micelles consist of a hydrophobic hydrocarbon core and more polar oxyethylene groups whose shapes only slightly differ from spherical symmetry. It has been found by electron spin resonance spectroscopy that the nitroxyl radicals are attached preferentially to specific atoms in the polyoxyethylene shell, *i.e.* the outer shell (~1.1 nm thickness) of the micelle (Wasserman, 1994). We prepared samples with 20 wt% of micelles in fully deuterated glycerol-water solutions. The object that is formed by the free radicals and the host molecule is then expected to give rise to a strong coherent SANS signal at smaller Q values than the TEMPO radical alone would give.

(3) The third class of sample we studied comprised solutions of monodisperse polystyrene nanospheres with a radius of several tens of nanometres embedded in a fully protonated glycerol-water solution which was doped with $2.5 \times 10^{19}\text{ cm}^{-3}$ complexes of EHBA-Cr^V. The average distance of the radicals for such a concentration is about 3.5 nm, which is much smaller than the radius of the nanospheres. Our intention was to 'design' a system that has, inside a polarizable matrix, large protonated areas free of paramagnetic centres (the polystyrene nanoparticles), which could allow one to directly observe spin diffusion into these areas.

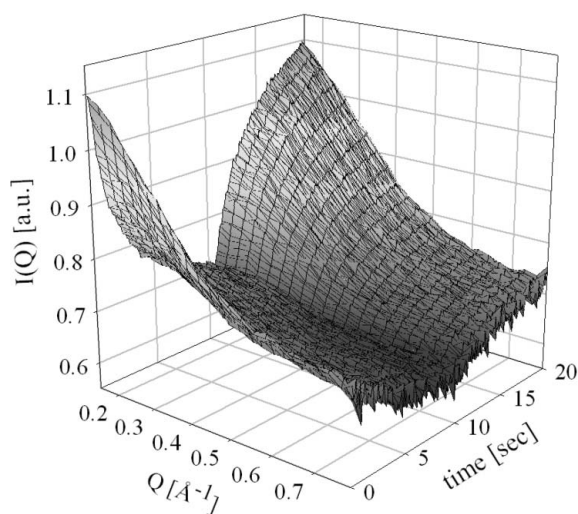


Figure 1
Time-dependent SANS intensity $I(Q)$ from a sample of 98% deuterated glycerol-water solution containing $5.0 \times 10^{19}\text{ cm}^{-3}$ EHBA-Cr^V (van den Brandt *et al.*, 2004).

All samples are based on a glycerol-water solution from which glassy slabs of about 3 mm thickness were obtained by injecting the solution into a copper mould pre-cooled to 77 K.

3. Stroboscopic small-angle neutron scattering

The SANS measurements were performed at the SANS instruments D22 at ILL (Grenoble, France), SANS-I at PSI (Kohlbrecher & Wagner, 2000) (Villigen, Switzerland), and PAPOL at LLB (Saclay, France). On all three instruments a time-resolved data-acquisition scheme was implemented. We used polarized incident neutrons of wavelengths $\lambda = 4.6\text{ \AA}$ (ILL), $\lambda = 4.7\text{ \AA}$ (PSI) and $\lambda = 8.0\text{ \AA}$ (LLB) and a respective wavelength spread of $\Delta\lambda/\lambda = 0.1$ (FWHM). The frozen samples were inserted into a NMR coil, placed in a microwave cavity, and mounted inside a ⁴He cryostat, which was operated at a temperature of about 1 K. A longitudinal static magnetic field of 3.5 T parallel to the incoming neutron beam direction was provided by a superconducting split coil (van den Brandt *et al.*, 2002). Samples could be changed and cooled down to 1 K in less than half an hour.

To create a transient polarization gradient, *i.e.* a polarization difference between protons close to a paramagnetic centre and those far away from them (bulk protons), we established a cyclic scheme where we polarized the sample continuously but changed the direction of the polarization periodically. The direction was reversed every 10 s for EHBA-Cr^V, every 20 s for the micellar systems and every 200 s for the nanospheres. This scheme is reasonably simple to implement and gives an optimum duty cycle. In parallel to the time-resolved acquisition of the SANS spectra (400 frames per full cycle), NMR spectra were taken, about one per second, to monitor the evolution of the bulk proton polarization. The SANS spectra taken during several hundred cycles were averaged to yield the scattering intensity for each time frame. For the background correction the polarization-dependent transmission was measured separately with the same cyclic procedure.

4. Experimental results

4.1. EHBA-Cr^V

The first successful experiments, which clearly showed that a polarization gradient between close and bulk protons can be established for a few seconds, were carried out in the EHBA-Cr^V system (van den Brandt *et al.*, 2002). As an example, Fig. 1 shows the cyclic (time-resolved) SANS intensity $I(Q)$ of EHBA-Cr^V in a 98% deuterated glycerol-water solution. The SANS intensity reflects the symmetry of the cyclic polarization procedure: during a single DNP cycle of 20 s duration, the nuclear spins are first polarized in one direction (0–10 s), then the microwave frequency is switched to the one which promotes polarization in the opposite direction (10–20 s). Several hundreds of such cycles have to be executed in order to collect data with sufficient statistics. As mentioned before, DNP allows one to change the value of the coherent nuclear scattering length of the proton and hence provides a means to vary the scattering-length density $\eta(t)$ of the EHBA-Cr^V molecule, which, in a continuum approximation, is of the general form $\eta(t) = a \pm bP(t)$. Analysis of the SANS data in Fig. 1 in terms of a core-shell model then provides information on the time dependence of the polarization P of the close protons. From the derived function $P(t)$ two characteristic time constants, τ_1 and τ_2 , could be extracted, which describe the dynamics of the polarization build-up of close and bulk protons (van den Brandt *et al.*, 2006).

The experiment was repeated with samples of different degrees of deuteration and different EHBA–Cr^V concentrations. We observed that τ_1 decreases while τ_2 increases with increasing protonation of the solvent, which can be understood within the framework of a two-reservoir model (van den Brandt *et al.*, 2006). In such a description the two heat reservoirs that are formed by the close and the bulk protons are coupled in series to the electron spin–spin reservoir.

The bulk proton polarization measured by NMR is also shown in Fig. 2. The difference in the time evolution of the polarization between close and bulk protons reflects the mechanism of DNP: a strong initial gradient develops due to a fast polarization of the protons close to the paramagnetic centre which then spreads out to the bulk with a slower rate.

4.2. TEMPO-doped C12E10 micelles

Evidence of a polarization gradient in the previous system has been found in a measurement of the temporal evolution of the close proton polarization with SANS. In the analysis, only the scattering contrast $\eta(t)$ was assumed to be time dependent but not the form factor itself. This is a reasonable assumption for molecules as small as EHBA–Cr^V, because all protons inside the molecule are still in the range of the dipole field of the unpaired electron. Nevertheless, a spin-diffusion gradient inside a large molecule can in principle also affect its Q -dependent form factor.

Such a molecule could be provided by a micelle that hosts the paramagnetic centres. We chose to study a sample of fully protonated C12E10 surfactant, with nominally six TEMPO radicals incorporated per micelle, prepared at a concentration of 20 wt% in a fully deuterated glycerol–water mixture. The sample was measured in a cyclic experiment with a time resolution of 0.1 s where every 20 s the direction of polarization was changed. An example of a measured scattering curve is shown in Fig. 3. It can be well described by a spherical shell model with a shell thickness of 1.1 nm and an overall radius of 2.6 nm, and an additional hard-sphere structure factor accounting for the high volume fraction (about 0.23) of micelles in the system. The time-dependent scattering signals were fitted taking, as for the EHBA–Cr^V system, the geometric dimensions of the micelle as global fit parameters. Only the polarization of the protons in the micelle and the incoherent background were assumed to be time dependent. The analysis showed that the assumption of a homo-

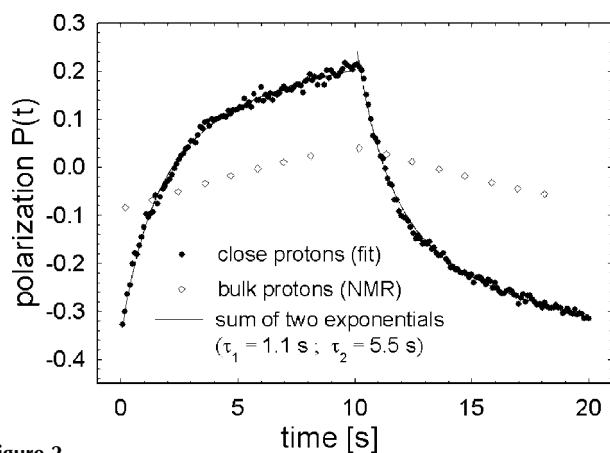


Figure 2 Close proton polarization deduced from the fit of the SANS data and the bulk proton polarization recorded by NMR. The polarization of the close protons could be described by the sum of two exponentials using the same weights (with opposite sign) and time constants for the two parts of the cyclic experiment (van den Brandt *et al.*, 2002).

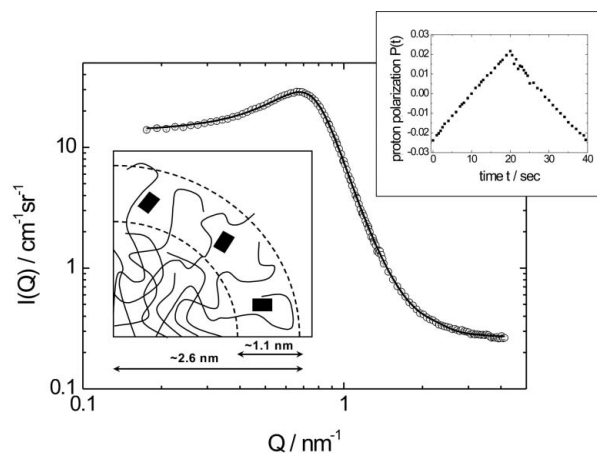


Figure 3 Scattering curve of C12E10 micelles in deuterated glycerol–water solvent. The insert shows a schematic sketch of the micelle structure and the position of the nitroxyl radicals (black rectangles) inside the micelle according to Clauss *et al.* (1993). The top right insert shows the time-dependent polarization of protons in micelles obtained by fitting the SANS data.

geneous polarization over the whole micelle at all times was already sufficient to describe the data within the error of the experimental data. The time-dependent polarization resulting from the fit is shown in the insert to Fig. 3. The fact that this model can already describe the data well enough suggests that within the micelle, which is about six times larger than the EHBA–Cr^V molecule, no polarization gradient could be seen. Even though the TEMPO molecules are located only in the shell of the micelle, the nuclear polarization seems to diffuse too fast into the core compared to the polarization speed of the shell, so that possible polarization gradients are too small to be detected with our method.

4.3. Undoped polystyrene nanospheres in an EHBA–Cr^V-doped glycerol–water matrix

In order to check whether the spin diffusion is indeed so fast and to possibly change the polarization speed, a third class of samples was studied. The system consists of monodisperse (protonated) poly-

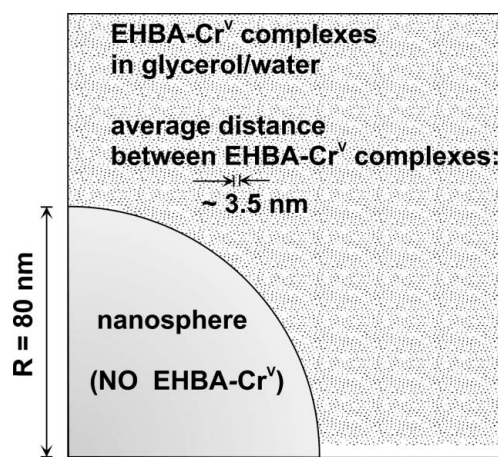


Figure 4 Sketch illustrating the length scales found in the sample investigated. The distance between the EHBA–Cr^V molecules is 40 times smaller than the diameter of the nanospheres. As the nanospheres do not contain any EHBA–Cr^V complexes, their protons will be polarized exclusively *via* the spin-diffusion process.

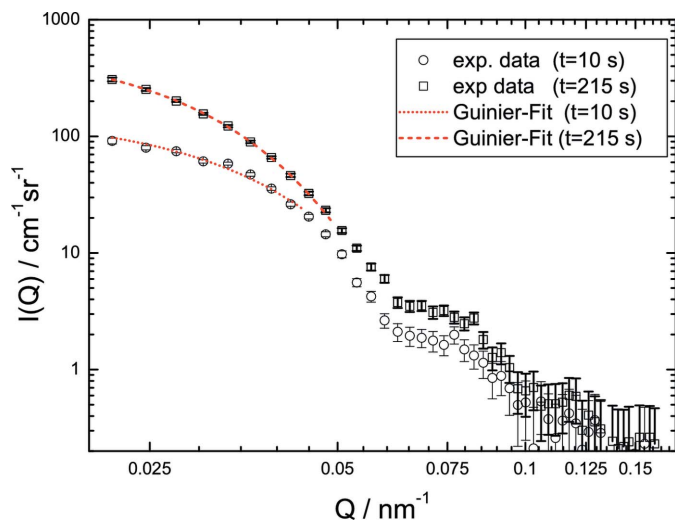


Figure 5
Selected scattering curves for 80 nm polystyrene nanospheres embedded in a EHBA-Cr^V doped glycerol-water matrix. Shown are the data for the two extreme cases, just after the switching of the polarization sign, with the fits to obtain the radius of gyration R_G .

styrene nanospheres (5 vol%) with a radius of 80 nm dissolved in a protonated glycerol-water solvent with a high concentration ($2.5 \times 10^{19} \text{ cm}^{-3}$) of EHBA-Cr^V complexes. The mean distance between the complexes is about 3.5 nm and therefore much smaller than the diameter of the nanospheres. The idea behind this system (see Fig. 4) is that the nanospheres exclude the radicals from a certain volume of the sample and provide well-defined protonated areas free of radicals. If we now start the DNP process only nuclei close to the paramagnetic centres get polarized, *i.e.* the protons in the glycerol-water matrix containing the EHBA-Cr^V complexes. All protons in the polystyrene nanospheres have to rely on spin diffusion to get polarized except for a small fraction close to the surface. The distance which has to be bridged by spin diffusion to reach the centre of a nanosphere is more than 30 times larger than in the micelle. This model system may allow one to study the polarization evolution on a much larger length scale.

In fact, we observe a change of the nanospheres' radius of gyration, R_G , which is correlated with the periodic switching of the sign of

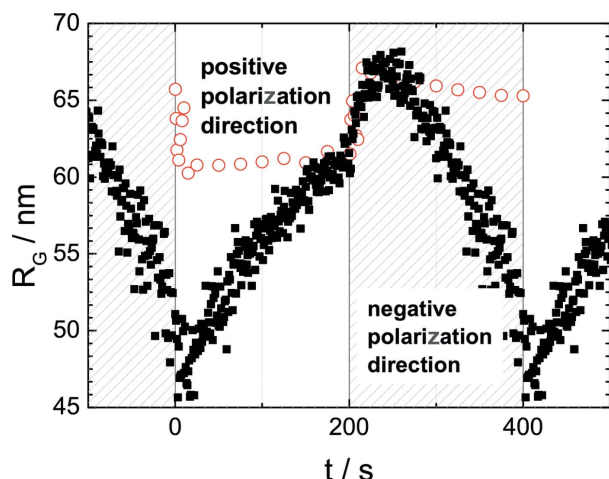


Figure 6
Change of the radius of gyration R_G during a cyclic SANS measurement. The filled black squares are experimental data and the open circles are obtained from the solution of equation (1), assuming a diffusion constant of $D = 800 \text{ nm}^2 \text{ s}^{-1}$.

polarization. The scattering curves for the two extreme cases, just after the microwave frequency switching, are shown in Fig. 5. The time dependence of R_G is then obtained by fitting the low- Q SANS data with $I(Q) = I_0 \exp(-R_G^2 Q^2/3)$ and is given in Fig. 6. It is clearly seen that R_G is changing strongly with time due to the development of a polarization gradient within the nanospheres.

The model-like character of the studied sample lends itself to a theoretical description. As the distance between the radicals is much smaller than the radius of the nanospheres, the polarization process can be approximated to the first order by a continuous model for which the partial differential equation for the polarization $P(t, r)$ can be written as

$$\frac{\partial P}{\partial t} = \begin{cases} D_{\text{sp}} \left(\frac{2}{r} \frac{\partial P}{\partial r} + \frac{\partial^2 P}{\partial r^2} \right) & \text{for } r \leq R \\ D_{\text{m}} \left(\frac{2}{r} \frac{\partial P}{\partial r} + \frac{\partial^2 P}{\partial r^2} \right) + \frac{P_0 - P}{\tau} & \text{for } r > R. \end{cases} \quad (1)$$

The term $(P_0 - P)/\tau$ is the source term which generates the polarization in the matrix *via* the DNP process up to a maximum P_0 . To take account of a change in the sign of the polarization build-up, only the sign of P_0 has to be changed, every 200 s in the present case. From NMR measurements we know that the saturation polarization $|P_0| = 0.25$ is reached exponentially with a time constant of $\tau = 248$ s. The first terms $D_{\text{sp,m}}[2/r(\partial P/\partial r) + (\partial^2 P/\partial r^2)]$ describe the spin diffusion in the sphere and the matrix, respectively. The spin-diffusion coefficients in the sphere D_{sp} and in the matrix D_{m} are assumed to be the same ($D_{\text{sp}} = D_{\text{m}} = D$) as the proton densities in both areas are very similar. In his classic textbook, Abragam provides an estimate for D of $10 \text{ nm}^2 \text{ s}^{-1}$ (Abragam, 1961), which seems very low. More recent NMR work finds much larger values for the diffusion rate: $800 \text{ nm}^2 \text{ s}^{-1}$ for polystyrene (Clauss *et al.*, 1993; Schmidt-Rohr & Spiess, 1994) and 530 and $710 \text{ nm}^2 \text{ s}^{-1}$, respectively, along the two principle axes of a CaF₂ single crystal (Zang & Cory, 1998).

In order to explain the experimentally found time-dependent radius of gyration (see Fig. 5), equation (1) has been solved numerically for different diffusion constants for a period of four cycles. Solving equation (1) yields $P(t, r)$ and therefore also the time-dependent scattering-length density profile, which then enables one to calculate the scattering cross section as well as the radius of

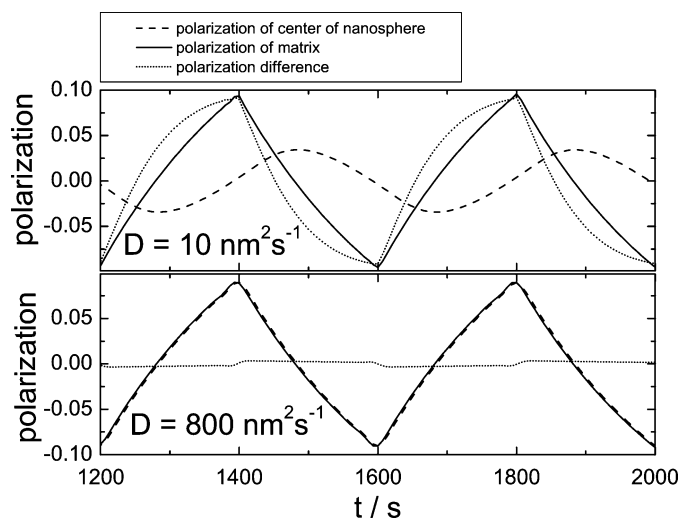


Figure 7
Time-dependent polarizations of the matrix and the centre of the nanosphere and their difference, as obtained by solving equation (1) numerically for $D = 800$ and $10 \text{ nm}^2 \text{ s}^{-1}$.

gyration (Fig. 6). The calculations show that a diffusion constant of $10 \text{ nm}^2 \text{ s}^{-1}$ would generate a very strong difference between the polarization in the centre of the nanosphere and the matrix, as shown in Fig. 7. For a diffusion coefficient of $800 \text{ nm}^2 \text{ s}^{-1}$ the polarization equalizes almost immediately, but nevertheless predicts a time-dependent radius of gyration which changes pronouncedly when the direction of polarization is reversed, as can be seen in Fig. 6. Even though the theoretical description of the spin-diffusion process into the nanosphere is still in progress, the experimental SANS data give strong evidence for a direct observation of a time-dependent polarization profile induced by dynamic nuclear polarization.

5. Discussion and conclusions

A prerequisite for the generation of a significant polarization gradient by the chosen method is that the rate of polarizing protons *via* paramagnetic centres is fast compared to the spin diffusion. This might be expressed in a general criterion

$$\sqrt{D\tau} \sim \ell, \quad (2)$$

where D is again the spin-diffusion coefficient, τ is the characteristic time constant for the polarization speed and ℓ is the characteristic size of the object in which a polarization gradient would be observed.

In the first system we studied the polarization evolution in EHBA-Cr^V complexes embedded in a highly deuterated environment. The mean distance between the protons within the complex is much shorter than the mean distance of the protons in the highly deuterated matrix. As the spin diffusion mainly depends on the distance between the protons, the border of the EHBA-Cr^V complex acts as a barrier for the spin diffusion. Therefore only a polarization gradient between the protons in the complex and in the solvent could be

established. The situation is slightly different for the micellar structure. The paramagnetic centres are embedded in the outer shell of the protonated micelles, whereas the matrix is again fully deuterated, thus the spin diffusion is fast inside the micelles and slow outside. But according to the above criteria the size of the micelle is still too small for the observation of a polarization gradient inside the micelle, which is supported by the SANS data. However, in the case of the nanospheres $\sqrt{D\tau}$ is not too large compared to their size, which allows one to observe a time dependence in the nanospheres' radius of gyration.

We would like to thank Dr V. K. Aswal for helping us in selecting and preparing a micellar system appropriate for the polarization experiment.

References

- Abragam, A. (1961). *Principles of Nuclear Magnetism*. Oxford University Press.
- Brandt, B. van den, Glättli, H., Grillo, I., Hautle, P., Jouve, H., Kohlbrecher, J., Konter, J. A., Leymarie, E., Mango, S., May, R. P., Stuhmann, H. B. & Zimmer, O. (2002). *Europhys. Lett.* **59**, 62–67.
- Brandt, B. van den, Glättli, H., Grillo, I., Hautle, P., Jouve, H., Kohlbrecher, J., Konter, J. A., Leymarie, E., Mango, S., May, R. P., Michels, A., Stuhmann, H. B. & Zimmer, O. (2004). *Nucl. Instrum. Methods A*, **526**, 81–90.
- Brandt, B. van den, Glättli, H., Grillo, I., Hautle, P., Jouve, H., Kohlbrecher, J., Konter, J. A., Leymarie, E., Mango, S., May, R. P., Michels, A., Stuhmann, H. B. & Zimmer, O. (2006). *Eur. Phys. J. B*, **49**, 157–165.
- Clauss, J., Schmidt-Rohr, K. & Spiess, H. W. (1993). *Acta Polym.* **44**, 1–17.
- Kohlbrecher, J. & Wagner, W. (2000). *J. Appl. Cryst.* **33**, 804–806.
- Schmidt-Rohr, K. & Spiess, H. W. (1994). *Multidimensional Solid-State NMR and Polymers*. London: Academic Press.
- Wasserman, A. M. (1994). *Russ. Chem. Rev.* **63**(5), 373–382.
- Zang, W. & Cory, D. C. (1998). *Phys. Rev. Lett.* **80**, 1324–1327.